

Study of silica-undersaturated magmas through the Kalsilite-Nepheline-Diopside-Silica system at 4.0 GPa and dry conditions

Estudo experimental de magmas alcalinos subsaturados em sílica por meio do sistema Kalsilita-Nefelina-Diopsídio-Sílica a 4.0 GPa e condições anidras

Márcio Roberto Wilbert de Souza¹, Rommulo Vieira Conceição¹,
Daniel Grings Cedeño¹, Roberto Vicente Schmitz Quinteiro¹

¹Instituto de Geociências, Universidade Federal do Rio Grande do Sul - UFRGS, Avenida Bento Gonçalves, 9.500, Agronomia, CEP 91501970, Caixa Postal 15001, Porto Alegre, RS, BR (rwsmarcio@gmail.com; rommulo.conceicao@ufrgs.br; dani_grings@hotmail.com; robertovsq@gmail.com)

Received on February 6, 2017; accepted on April 27, 2018

Abstract

This study experimentally investigates the Kalsilite-Nepheline-Diopside-Silica system at high pressure and temperature, with emphasis on silica-undersaturated volume (leucite-nepheline-diopside — Lct-Nph-Di; and kalsilite-nepheline-diopside — Kls + Nph + Di — planes), at 4.0 GPa (~120 km deep), temperatures up to 1,400°C and dry conditions, to better understand the influence of K₂O, Na₂O, and CaO in alkali-rich silica-undersaturated magma genesis. In the Lct-Nph-Di plane, we determined the stability fields for kalsilite (Kls_{ss}), nepheline (Nph_{ss}) and clinopyroxene (Cpx_{ss}) solid solutions, wollastonite (Wo) and sanidine (Sa); and three piercing points: (i) pseudo-eutectic Kls + Nph + Di + liquid (Lct₆₂Nph₂₉Di₉) at 1,000°C; (ii) Kls + Sa + (Di + Wo) + liquid (Lct₇₅Nph₂₂Di₂) at 1,200°C; and (iii) pseudo-eutectic Kls + Di + Wo + liquid (Lct₇₄Nph₁₇Di₉) at 1,000°C. Kalsilite stability field represents a thermal barrier between ultrapotassic/potassic vs. sodic compositions. In the plane Kls-Nph-Di, we determined the stability fields for Kls_{ss}, Nph_{ss} and Cpx_{ss} and two aluminous phases in smaller proportions: spinel (Spl) and corundum (Crm). This plane has a piercing point in Kls + Nph + Di(± Spl) + liquid (Kls₄₇Nph₄₃Di₁₀) at 1,100°C. Our data showed that pressure extends K dissolution in Nph (up to 39 mol%) and Na in Kls (up to 27 mol%), and that these solid solutions, if present, determinate how much enriched in K and Na an alkaline magma will be in an alkaline-enriched metasomatic mantle. Additionally, we noted positive correlation between K₂O and SiO₂ concentration in experimental melts, negative correlation between CaO and SiO₂, and no evident correlation between Na₂O and SiO₂.

Keywords: Experimental petrology; Alkaline rocks; Potassium; Mantle.

Resumo

Este trabalho trata do estudo experimental do sistema kalsilita-nefelina-diopsídio-sílica em condições mantélicas, com ênfase em sua parte subsaturada em sílica (planos leucita-nefelina-diopsídio — Lct-Nph-Di; e kalsilita-nefelina-diopsídio — Kls + Nph + Di), a 4 GPa (profundidade de aproximadamente 120 km), até 1.400°C em condições anidras. O objetivo é melhor compreender como K₂O, Na₂O e CaO influenciam a gênese de magmas ricos em álcalis e subsaturados em sílica. Para o plano Lct-Nph-Di, foram determinados campos de estabilidade para as soluções sólidas kalsilita (Kls_{ss}), nefelina (Nph_{ss}) e clinopiroxênios (Cpx_{ss}), além de wollastonita (Wo) e sanidina (Sa). Foram também definidos os pontos invariantes: (i) pseudoeutético Kls+Nph+Di+líquido (Lct₆₂Ne₂₉Di₉) a 1.000°C; (ii) Kls + Sa + (Di + Wo) + líquido (Lct₇₅Nph₂₂Di₂) a 1.200°C; (iii) pseudoeutético Kls + Di + Wo + líquido (Lct₇₄Nph₁₇Di₉) a 1.000°C. O campo da kalsilita, nesse diagrama, representa um alto termal entre os extremos composicionais potássico/ultrapotássico vs. sódico. No plano Kls-Nph-Di, encontramos campos de estabilidade para Kls_{ss}, Nph_{ss} e Cpx_{ss}, além de pequenas quantidades de espinélio (Spl) e corindon (Crm) e um ponto pseudoeutético Kls + Nph + Di(± Spl) + líquido (Kls₄₇Nph₄₃Di₁₀) a 1.100°C. Os dados sugerem que o aumento de pressão estende a dissolução de K em Nph (até 39% molar) e de Na em Kls (até 27% molar). Quando presentes, essas soluções sólidas determinam quão ricos em K ou Na serão os magmas gerados nesses sistemas. Adicionalmente, foram vistas correlações positivas entre as concentrações de K₂O e sílica nos líquidos silicáticos gerados experimentalmente, negativas entre CaO e sílica e nenhuma relação direta entre Na₂O e sílica.

Palavras-chave: Petrologia experimental; Rochas alcalinas; Potássio; Manto.

INTRODUCTION

The processes and environments related to the genesis of alkaline rocks on Earth have been an active theme among geologists over the last few decades. Yoder and Tilley (1962), using the concept of the basalt tetrahedron, determined the clinopyroxene (Cpx) \pm nepheline (Nph) \pm forsterite (Fo) \pm silica system, to better understand the compositions of the liquids in equilibrium with the final steps of alkali basalts crystallization. Such work influenced Sood et al. (1970) to elaborate the diopside (Di) \pm nepheline \pm kalsilite (Kls) \pm silica system, a tetrahedron that comprises the majority of alkaline rocks compositions, highlighting potassium, sodium, and calcium in its vertices. After that, the concentration of the elements K, Na and Ca and their ratios have been used in the classification of the alkaline rock groups (Foley et al., 1987; Le Maitre, 2002), but exactly how much each of them influences the genesis and the characteristics of alkaline magmas is still a debated issue.

Current geochemical and isotopic studies show that alkaline rocks can be originated through partial melting of primitive assemblages (from mantle sources) enriched in alkalis via several metasomatic processes, like interaction with volatile-rich fluids or silicate liquids originated from partial melting of subducting slabs (Conceição et al., 2000; Conceição and Green, 2004; Bea et al., 2013; Condamine and Ménard, 2014; Laporte et al., 2014). Moreover, the presence of carbonates, mica (phlogopite) and/or amphiboles (pargasite, richterite) in peridotite xenoliths carried by alkaline magmas (like alkali basalts, kimberlites or lamproites) denotes the role of H₂O and CO₂ (C–H–O system) generically lowering temperatures needed to magma generation (Conceição and Green, 2000, 2004).

In order to understand the role of K₂O, Na₂O, and CaO in the mantle composition to the genesis of alkaline magmas, several experimental studies have been conducted using simple systems (between two and four components) as analogues for natural rocks, determining the solidus and near-solidus melt compositions in a wide range of pressure and temperature conditions (Gupta and Lidiak, 1973; Edgar et al., 1976; Gupta and Green, 1988; Mengel and Green, 1989; Wallace and Green, 1991; Draper and Green, 1999; Conceição and Green, 2000, 2004; Gupta et al., 2006, 2010).

With the aim of comprehending the influence of K₂O concentration on silica activity in alkaline magmas, Conceição and Green (2000) simulated a K-rich olivine–leucite–quartz system in dry conditions, at 0.5 to 2.0 GPa and varied temperatures. Their results suggest that K-rich silica-oversaturated magmas (with very low Na₂O content), with minor contents of water and CO₂, could be produced by partial melting of potassic-harzburgite or phlogopite-bearing lherzolite, at pressures of up to nearby 2 GPa and temperatures between 1,200 and 1,300°C. For alkaline silica-undersaturated magma production, however, partial melting of a potassium enriched mantle (lherzolite or harzburgite) needs pressure and temperature higher than 2.0 GPa and 1,200°C,

respectively, favored by the presence of CO₂ or fluorine. Walter and Presnal (1994) studied the Na₂O and CaO relations on alkaline magmas and their influence on the silica concentration in these liquids. They showed, through experimental studies, that sodic systems at ≥ 1 GPa produce silica-undersaturated melts, while calcic systems at the same pressure produce just silica-saturated melts, both in anhydrous conditions.

Conceição and Green (2000) and Walter and Presnal (1994) analyzed sodic and potassic systems separately in their experiments. Using another approach, Gupta and Lidiak (1973) studied the silica-substituted join Lct–Nph–Di at 1 atm, testing variable concentrations of K₂O and Na₂O. In such work, they determined the stability fields for the nepheline, leucite, diopside and forsterite solid solutions. This way, they produced a leucite bearing wehrlite (piercing point Lct+Di+Fo at 1,280°C), and determined the eutectic Nph₂₉ + Di₂₇ + Lc₇₇ at $\sim 1,200^\circ\text{C}$ (Figure 1). In recently investigation, Gupta et al. (2006) studied the Sa + Nph + Di silica-undersaturated system at 1 and 2 GPa with $P(\text{H}_2\text{O}) = P_{\text{total}}$ in order to determine the stability fields of diopside, nepheline, and sanidine. Then, they found the eutectic Nph₃₁ + Sa₆₅ + Di₄ at 670°C and 1 GPa, and the eutectic Nph₂₄ + Sa₇₃ + Di₃ at 640°C and 2 GPa, which shows a slight shift of the eutectic to the K-rich field (Sa vertex) through pressure increasing.

K₂O, Na₂O and CaO mantle source concentration

No specific values are determined for the concentrations of alkaline elements for the Earth's mantle, which vary accordingly to the preferred model. Lyubetskaya and Kurenaga (2007) postulate that the concentration of alkalis for the primitive Earth's mantle (in wt%) is: 2.79 ± 0.47 for CaO; 0.298 ± 0.141 for Na₂O; and 0.023 ± 0.005 for K₂O. McDonough and Sun

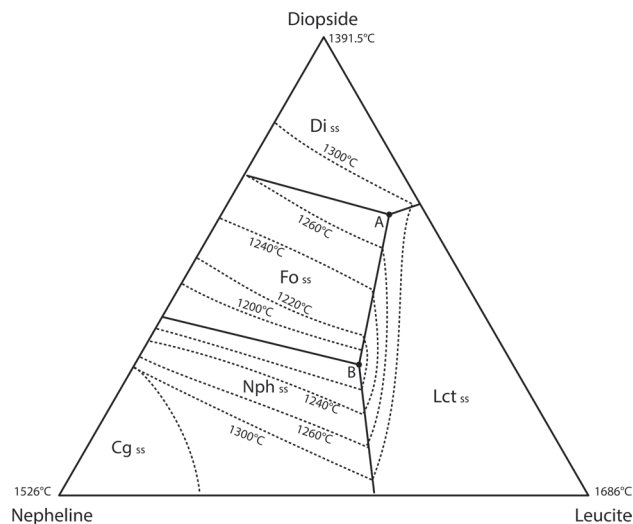


Figure 1. Phase diagram leucite-nepheline-diopside (Lct–Nph–Di), at 1 atm and dry conditions, after Gupta and Lidiak (1973).

(1995) estimate 3.53 ± 0.35 for CaO; 0.359 ± 0.054 for Na₂O; and 0.029 ± 0.06 for K₂O. Concentrations in enriched mantle are even more difficult to estimate, due to its great heterogeneity. However, Menzies and Hawkesworth (1987) describe metasomatized lherzolites in which K₂O exceeds 1%, which could represent its abundances in a metasomatized mantle.

Although concentrations for Na and K are considered relatively low in the mantle as a whole, there are evidences for the presence of such elements in the deep mantle, such as inclusions of (Na,K)-hollandite in diamonds produced by melting of pelagic metasediments, carried to deep mantle depths via ancient subducted oceanic slabs (Plá Cid et al., 2014). Carniel et al. (2014) demonstrated that pelagic K-rich smectites play a major role carrying potassium to deep Earth via subduction. This sediment input can represent an important source of potassium, not only to the mantle wedge, but also to the whole Earth's mantle.

Potassium is an element of special interest in the mantle. Beyond its contribution for the K-enriched magmas genesis and their associated mineralization (as diamond, gold and rare Earth elements), it is also important as a heat source to the Earth's mantle, due to the ⁴⁰K isotope "fast" decay (1.25 Ga half-life), compared to the ²³⁵U and ²³²Th contributions (half-life of 4.5 Ga and 14.05 Ga, respectively) (Jaupart et al., 2007; Arevalo et al., 2009).

Objectives of this study

In this work, we performed experiments at 4.0 GPa (~120 km deep) of pressure and temperatures up to 1,400°C, in the silica-undersaturated part of the diopside-nepheline-kalsilite-silica tetrahedron (CMANKS system), emphasizing the Lct-Nph-Di and Kls-Nph-Di planes, at anhydrous conditions, in order to discriminate the role of K₂O, Na₂O and CaO in parameters like silica saturation of melts, derived from sodium- and potassium-enriched mantle. In order to achieve that, we started with compositions similar to the ones studied by Gupta and Lidiak (1973) on the system Di + Nph + Lct, at 1 atm and dry conditions. With higher pressures, in relation to previous work, we could better understand the genesis of some silica-undersaturated melts, like nepheline-bearing phonolites, and

determinate the crystalline phases produced in such conditions and their petrologic implications. Although mica- and/or amphibole-bearing mantle rocks are commonly accepted as the source of alkaline magmas (Conceição and Green, 2004; Condamine and Ménard, 2014; Laporte et al., 2014), we performed water-free experiments in order to better focus on the role of K₂O, Na₂O, and CaO (water would represent another variable, reducing the melting point of the compositions, which would deviate from the objective of this work). Up to now, there are no studies neither for the Lct-Ne-Di nor for the Kls-Ne-Di joins at 4.0 GPa or higher pressures.

METHODOLOGY

Starting materials

The starting materials were prepared based on the method described by Conceição and Green (2004). Mixtures of carbonates (CaCO₃, MgCO₃, Na₂CO₃, and K₂CO₃) and oxides (Al₂O₃ and SiO₂) were produced aiming to synthesize glasses with diopside (CaMgSi₂O₆), nepheline (NaAlSi₃O₈), kalsilite (KAlSi₃O₈), and leucite (KAlSi₂O₆) stoichiometric compositions (the vertices of the diagrams). These mixtures were simultaneously decarbonated (to release CO₂) and sintered at 1,000°C for ~24 hours, before being ground in an agate mortar with acetone, to complete homogenization. After that, the mixtures were melted in a high temperature furnace at 1,350°C for 30 minutes in a platinum crucible, and then quickly poured and cooled into a cold stainless-steel plate. Each produced glass was then grounded in an agate mortar with acetone and stored in an oven at 110°C to be kept dry. All glasses were analyzed by X-ray diffraction (XRD) to ensure complete amorphization of the material after melting, and scanning electron microscopy with energy dispersive X-ray spectroscopy (SEM-EDS) analysis was performed to determinate if glass composition had no variation after melting (Table 1). SiO₂ content in Leucite glass increased almost 5 wt% in relation to its initial calculated composition. As experiments were made by mixtures of leucite, nepheline

Table 1. Energy dispersive spectroscopy broad area analysis for the produced glasses (G-Kls, G-Lct, G-Nph, G-Di). C-Kls, C-Lct, C-Nph and C-Di columns shows previously calculated wt% oxide stoichiometric composition.

%wt	G-Kls	C-Kls	G-Lct	C-Lct	G-Nph	C-Nph	G-Di	C-Di
SiO ₂	35.75	37.99	50.12	55.06	43.61	42.29	56.25	55.5
Al ₂ O ₃	33.17	32.23	24.91	23.36	36.35	35.89	0.01	0
MgO	0.02	0	0.03	0	0.01	0	16.92	18.61
CaO	0.02	0	0.02	0	0.01	0	26.75	25.89
K ₂ O	30.73	29.78	24.91	21.57	0.02	0	0.04	0
Na ₂ O	0.3	0	0.03	0	20	21.81	0.02	0
Total	99.99	100	100.02	99.99	100	99.99	99.99	100

G-Kls: kalsilite glass; C-Kls: calculated kalsilite; G-Lct: leucite glass; C-Lct: calculated leucite; G-Nph: nepheline glass; C-Nph: calculated nepheline; G-Di: diopside glass; C-Di: calculated diopside.

and diopside glasses, this SiO₂ increased difference was diluted in the bulk samples and it was considered not relevant to take significant changes in overall experiments stoichiometry.

Initial samples used in the experiments were mixtures with different proportions of the produced glasses. The proportions were calculated depending on the area of interest in the phase

diagrams. As little variations in the initial sample compositions can occur during its preparation, SEM-EDS broad area analyses were performed after each experimentation to precisely determine the initial sample compositions (Table 2). Platinum capsules were used in the experiments due to its inert characteristic and high fusion temperature, preventing interaction with samples.

Table 2. Average energy dispersive spectroscopy broad area analysis for the leucite-nepheline-diopside (Lct-Nph-Di) and kalsilite-nepheline-diopside (Kls-Nph-Di) systems experiments, representing the precise initial compositions.

Lct-Nph-Di system										
	Na ₂ O	MgO	Al ₂ O ₃	SiO ₂	K ₂ O	CaO	Total	Leucite	Nepheline	Diopside
402	4.45	10.91	15.46	49.06	2.58	17.55	100.00	13.10	17.15	69.75
STD	0.17	0.36	0.64	0.24	0.24	0.48				
403	3.01	2.85	22.37	52.50	14.31	4.96	100.00	70.34	11.25	18.41
STD	0.13	0.20	0.25	0.21	0.19	0.34				
403II	3.19	3.36	21.95	52.26	13.57	5.66	100.00	66.73	11.92	21.35
STD	0.15	0.15	0.18	0.18	0.33	0.23				
404	16.97	1.96	31.53	43.49	3.09	2.96	100.00	16.83	70.17	0.10
STD	0.23	0.16	0.30	0.22	0.08	0.23				
405	11.50	2.87	27.10	47.14	6.24	5.16	100.01	33.15	46.44	20.41
STD	0.09	0.04	0.06	0.06	0.09	0.11				
406	1.95	52.42	10.66	9.19	3.64	22.13	100.00	17.62	7.19	75.19
STD	0.33	0.05	1.39	0.47	0.68	2.40				
406II	2.42	12.60	8.82	52.36	3.50	20.31	100.00	16.49	8.65	74.86
STD	0.055	0.085	0.045	0.03	0.03	0.08				
407	4.39	8.30	16.08	51.40	6.21	13.63	100.00	30.87	16.58	52.55
STD	0.07	0.17	0.23	0.06	0.15	0.26				
409	6.81	10.39	14.97	49.63	1.92	16.28	100.00	9.60	25.88	64.52
STD	0.77	0.56	0.81	0.16	0.28	1.31				
413	2.67	12.93	8.45	52.38	3.14	20.44	100.00	14.73	9.53	75.75
STD	0.20	0.67	0.81	0.14	0.64	0.84				
415	8.05	9.53	16.41	48.83	2.30	14.87	100.00	11.37	30.25	58.39
STD	0.28	0.31	0.47	0.17	0.17	0.44				
Kls-Nph-Di system										
	Na ₂ O	MgO	Al ₂ O ₃	SiO ₂	K ₂ O	CaO	Total	Leucite	Nepheline	Diopside
k402	9.57	2.28	33.56	38.79	11.47	4.33	100.00	35.48	44.83	19.70
STD	0.16	0.02	0.23	0.19	0.14	0.10				
k403	1.39	11.98	14.21	48.11	5.07	19.25	100.00	12.42	5.40	82.18
STD	0.04	0.65	0.72	0.27	1.37	1.03				
k404	1.52	10.91	16.53	47.43	5.55	18.07	100.00	13.97	6.19	79.84
STD	0.09	0.50	0.77	0.24	0.57	0.70				
k405	5.84	10.96	16.04	48.30	1.33	17.53	100.00	3.52	23.52	72.95
STD	0.06	0.06	0.21	0.13	0.01	0.13				

STD: standard deviation.

Experiments

The high pressure and temperature experiments were conducted at the High Pressure and Advanced Material Laboratory at Federal University of Rio Grande do Sul (LAPMA-UFRGS), using a 1,000 tnf hydraulic press coupled with toroidal profile chambers. This configuration allows a homogeneous distribution of pressure during experiments. With this apparatus, experiments can reach pressures up to 7.7 GPa and temperatures up to 2,000°C. As all experiments in this study were conducted at 4.0 GPa, pressure calibrations were performed using metallic ytterbium (Yb), which has a phase transition at this pressure. Experimental run times were 8 hours. Experiments performed in the described apparatus had pressure and temperature accuracies of ± 0.5 GPa and $\pm 25^\circ\text{C}$, respectively (Carniel et al., 2014). Some experiments were performed twice to verify the reproducibility of this methodology.

The pressure cell consists of a graphite heater, which encloses a hexagonal boron nitride sleeve (a soft material that helps to distribute pressure homogeneously), which comprises the platinum capsule containing the sample. Above and below the hexagonal boron nitride sleeve, two calcinated pyrophyllite disks were placed as temperature insulators. The Pt capsules were filled with sample and welded to seal it, reaching a cylindrical form with 5 mm diameter and 4 mm height. Loaded capsules were weighted before and after being welded to ensure no material loss during experimentation. The entire configuration was placed into a toroidal gasket (made of CaCO₃, Al₂O₃, and polyvinyl acrylate), which was placed between the toroidal plates.

In all experiments, pressure was gradually applied at room temperature, until it reached 4.0 GPa. After that, the 4.0 GPa pressure was kept 15 minutes at room temperature for system stabilization before heating starts. For each experiment, temperature was increased slowly up to 100°C higher than the desired value for 30 minutes. After that, temperature was lowered to the target condition. Temperature was measured *in situ* with a type-B thermocouple (Pt-Pt₈₇Rh₁₃) encapsulated in Al₂O₃ sleeves. At the end of each experiment, temperature was turned off. Quench rate is estimated to be 200°C/min, which guarantees a drop of temperature of 200 to 400°C right after ending the experiment. Each experiment product was mounted in epoxy resin and sectioned in half: one part went to SEM-EDS analysis, and the other part was powdered in an agate mortar for XRD analysis.

Analytical procedures

Experimental run products were analyzed by two techniques: XRD, at LAPMA-UFRGS; and SEM-EDS, at Isotopic Geology Laboratory (LGI) of Geosciences Institute (IGeo), at UFRGS. A few samples were either analyzed by wavelength-dispersive spectroscopy (WDS) electron microprobe

for comparison with energy dispersive spectroscopy (EDS) data, and no relevant variation was found between the two techniques. However, WDS analysis showed lower potassium loss (up to 1 wt%) and lower standard deviation.

XRD analyses were conducted to determine the mineral crystallized in each experiment. A Siemens D500 XRD powder diffractometer equipped with a CuK α source and a graphite monochromator in the secondary beam was used. The diffractograms of all samples were obtained from 5 to 80° with a step of 0.05° and acquisition time of 0.5 s/step.

SEM-EDS analyses were used to establish compositions of each phase in the experiments (melt and crystalline phases). SEM was also applied for elemental mapping (as help tool on data interpretation, but it was not presented in this article), and back-scattered/secondary electron imaging. A JEOL-6610LV was used, with accelerating voltage of 15 kV, specimen current of 10 nA and spot size of ca. 1 μm (voltage and specimen current by Conceição and Green, 2004). A curve of counting time and K- and Na-loss was made, and counting times of 60 s were used to reduce K and Na loss by volatilization.

RESULTS AND INTERPRETATIONS

Experimental results for melt and crystalline phase compositions are summarized in Tables 3 and 4. Figures 2 and 5 are phase diagrams showing stability fields for the produced phases in our experiments. X-ray diffraction (Figure 4) aid the identification of crystalline phases in the experiments.

Quality of the experiments

Our experiments were designed to produce large pools of melt in equilibrium with all mineral phases in each experiment. In all experiments, homogenization of each phase composition is assured by the low standard deviation on average analysis. For the determination of the *liquidus* phase composition, analysis was run in broad area, to prevent K and Na loss.

The good quality of our experiments was verified by the euhedral habit of the produced crystals, absence of either compositional zonation in minerals and/or skeletal crystals in the runs. These features showed that phases in our experiments were in equilibrium among them, and that the quench was efficient. The experiments run time was tested based on the equilibrium among phases and was set for 8 hours. Some experiments (403, 406) were performed twice to warrantee reproducibility, and no significant changes were found between original experiments and their duplicates. The standard deviation of the analyzed phases was minimal (Tables 3 and 4), which ensure the high quality of our experiments.

Table 3. Experimental temperature and produced phases for leucite-nepheline-diopside (Lct-Nph-Di) phase diagram, at 4.0 GPa and anhydrous condition (scanning electron microscopy with energy dispersive X-ray spectroscopy analyzes). Pyroxene shows end members (Di and Jd) between parentheses. Normalized values for melt compositions (Lct, Nph and Di) are plotted in phase diagram (Figure 2).

Experiment Phase	T°C	Crystalline products	Composition wt%						Position in the diagram			
			Na ₂ O	MgO	Al ₂ O ₃	SiO ₂	K ₂ O	CaO	Total	Lct	Nph	Di
402												
Melt	1,000	Di+Kls+Nph	6.23	0.89	25.39	55.15	10.23	2.11	100.00	62.48	28.92	8.59
STD			0.27	0.05	0.16	0.29	0.31	0.08				
Di (Di94Jd6)			1.59	14.87	9.91	50.12	0.00	23.50	100.00			
STD			0.54	0.74	1.72	0.82	0.00	0.89				
Kls			5.22	0.21	33.26	39.48	21.53	0.32	100.02			
STD			0.14	0.04	0.19	0.19	0.13	0.06				
Nph			13.07	0.57	33.48	41.27	10.99	0.62	100.00			
STD			0.14	0.22	0.49	0.60	0.36	0.27				
403												
Melt	1,200	Di+Kls+Sa	3.63	0.64	25.10	57.91	11.65	1.07	100.00	76.48	18.10	5.42
STD			0.01	0.01	0.01	0.02	0.02	0.01				
Di (Di90Jd10)			1.46	15.68	7.09	51.76	0.19	23.81	100.00			
STD			0.28	0.75	1.97	0.92	0.13	0.74				
Sa			0.85	0.02	19.86	64.64	14.23	0.41	100.00			
STD			0.03	0.01	0.35	0.26	0.16	0.05				
Kls			2.59	0.10	32.90	39.21	24.90	0.30	100.00			
STD			0.01	0.02	0.11	0.25	0.16	0.01				
403II												
Melt	1,200	Di+Kls+Sa	4.33	0.26	24.82	57.38	12.54	0.66	100.00	77.10	20.25	2.65
STD			0.13	0.02	0.13	0.29	0.33	0.07				
404												
Melt	1,400	Omp+Nph	sub	-	-	-	-	-	-	-	-	-
Omp (Di57Jd43)			6.32	9.69	16.95	51.12	0.12	15.80	100.00			
STD			0.44	0.42	1.20	0.95	0.07	0.47				
Nph			18.64	0.29	35.38	41.58	3.74	0.41	100.04			
STD			0.73	0.11	0.45	1.09	0.16	0.06				
405												
Melt	1,200	Omp+Nph	sub	-	-	-	-	-	-	-	-	-
Omp (Di44Jd56)			8.40	6.05	19.95	53.59	0.55	11.46	100.00			
STD			0.39	0.29	0.19	1.04	0.15	0.97				
Nph			14.22	0.10	34.91	40.29	10.16	0.34	100.01			
STD			0.13	0.04	0.13	0.07	0.08	0.04				
406												
Melt	1,000	Di+Kls+Wo	3.54	0.08	23.20	59.22	11.01	2.95	100.00	73.46	17.94	8.60
STD			0.65	0.05	0.10	0.57	0.95	0.23				
Di (Di93Jd7)			0.95	17.63	4.25	52.79	0.02	24.37	100.00			
STD			0.06	0.21	0.32	0.18	0.02	0.12				
Kls			2.31	0.24	32.39	39.04	25.02	1.01	100.00			
STD			0.01	0.35	0.62	0.51	0.90	0.65				
Wo			0.46	1.81	1.64	49.33	0.28	46.49	100.00			

Continue...

Table 3. Continuation.

Experiment Phase	T°C	Crystalline products	Composition wt%						Position in the diagram			
			Na ₂ O	MgO	Al ₂ O ₃	SiO ₂	K ₂ O	CaO	Total	Lct	Nph	Di
STD			0.22	1.29	0.59	0.24	0.18	2.00				
406II												
Melt	1,000	Di+Kls+Wo	3.55	0.38	21.88	59.14	11.22	3.83	100.00	71.24	17.14	11.62
STD			0.04	0.18	0.11	0.06	0.18	0.10				
407												
Melt	1,300	Di	5.41	1.51	23.95	53.84	9.94	5.35	100.00	57.86	23.91	18.23
STD			0.11	0.06	0.08	0.19	0.13	0.10				
Di (Di87Jd13)			1.28	16.80	4.03	53.12	0.00	24.76	100.00			
STD			0.14	0.38	0.78	0.34	0.00	0.34				
409												
Melt	1,300	Di	11.85	2.17	25.31	49.36	5.25	6.05	100.00	29.07	49.83	21.10
STD			0.23	0.06	0.36	0.30	0.05	0.06				
Di (Di89Jd11)			1.83	15.40	8.06	51.03	0.00	23.67	99.99			
STD			0.12	0.44	1.03	0.54	0.00	0.23				
413												
Melt	1,200	Di+Kls	6.42	1.22	19.60	52.19	13.76	6.80	100.00	61.96	21.97	16.07
STD			0.15	0.10	0.08	0.15	0.22	0.42				
Di (Di89Jd11)			1.59	15.80	6.43	51.89	0.32	23.97	100.00			
STD			0.26	0.72	1.41	0.72	0.27	0.57				
Kls			2.78	0.30	32.41	39.22	25.09	0.20	100.00			
STD			0.20	0.03	0.11	0.20	0.17	0.07				
415												
Melt	1,200	Di+Nph	15.41	3.07	19.50	50.07	5.77	6.17	99.99	26.41	53.55	20.05
STD			0.69	0.42	0.97	1.43	0.46	0.62				
Omp (Di57Jd43)			2.78	14.67	8.57	51.90	0.02	22.07	100.01			
STD			0.26	0.40	1.23	0.80	0.00	0.24				
Nph			16.78	0.45	34.36	41.08	7.15	0.20	100.02			
STD			0.05	0.04	0.14	0.17	0.08	0.01				

STD: standard deviation; Sa: salinite; Omp: omphacite; Wo: wollastonite.

Leucite-nepheline-diopside diagram at 4.0 GPa and dry condition

Stability fields for sanidine (Sa), kalsilite, nepheline, wollastonite (Wo) and clinopyroxene, together with piercing points and cotectic lines for the Lct-Nph-Di system are given in Figure 2 (all mineral abbreviation from Whitney and Evans, 2010). Experimental conditions and products composition are given in Table 3. Kalsilite, nepheline and clinopyroxene are solid solutions. Cpx_{ss} composition vary from diopside (Di — calcic) to omphacite (Omp — when the jadeite [Jd] component is higher than 20%) closer to nepheline vertex (experiments 404, 405 and 415). Classification and nomenclature of pyroxenes are after Morimoto (1989). Three four-phase piercing points were determined in the Lct-Nph-Di phase diagram: the Kls + Nph + Di plus a

liquid (Lc₆₂Ne₂₉Di₉) at 1,000°C; the Kls + San + Di plus liquid (Lct₇₆Nph₁₈Di₆) at 1,200°C; and the Kls + Di + Wo plus liquid (Lct₇₃Nph₁₈Di₉) at 1,000°C.

Comparing our data to the ones reported in Gupta and Lidiak (1973) and Singh et al. (2000), who studied the Nph-Di-Kls and Di-Nph systems, respectively, both under dry conditions, the stability of olivine decreases progressively with pressure increasing in an alkaline enriched system. Gupta and Lidiak (1973) found olivine at 1 atm and temperature up to 1,280°C, while Singh et al. (2000) found it at 0.1 GPa and temperature up to 950°C. At 4.0 GPa (this study) olivine stability field is absent in a potassium-, sodium- and calcium-enriched environment. On the other hand, clinopyroxene stability field grows and includes the solid solution composition to omphacite (Di₄₄₋₅₇Jd₅₆₋₄₃) near Nph field in the diagram. Our Cpx and Omp showed values for K₂O up to 0.12 wt% (experiment 403). In opposition to Luth (1997),

Cpx in our study did not present significant K₂O content, in the absence of K-rich phases (experiment 415).

The products of experiment 402 represent a pseudo-eutectic (Lc₆₂Nph₂₉Di₉), in which kalsilite, nepheline and diopside (Di₉₄Jd₆) solid solutions are in equilibrium with liquid at 1,000°C (Figure 3A). This point is near the boundary between sodic and potassic fields in the phase diagram. Both Kls and Nph have hexagonal structure (Klein and Dutrow, 2007), and have a limited range for Na-K solid solution. The existence of a pseudo-eutectic with these minerals is

consistent with results shown in Schairer (1950), who first determined the Nph-Kls-SiO₂ phase diagram at 1 atm, and Gupta and Lidiak (1973) (Lct-Nph-Di at 1 atm phase diagram). Gupta et al. (2010) studied the Kalsilite-Nepheline-Silica system at 2 GPa and stated that Nph can carry up to 28.7% of Kls in its structure, while Kls carries only 12.4% of Nph. Our data suggests that the solubility of potassium in nepheline and sodium in kalsilite is higher if pressure is up to 4.0 GPa. At this pressure, Nph can carry up to 35 mol% of Kls in its structure, while Kls carries up to 26.9 mol% of Nph.

Table 4. Experimental temperature and produced phases for kalsilite-nepheline-diopside (Kls-Nph-Di) phase diagram, at 4.0 GPa and anhydrous condition (energy dispersive X-ray spectroscopy analyses). Pyroxenes end-members (Di and Jd) in parenthesis. Normalized values for melt compositions (Kls, Nph and Di) are plotted in phase diagram in Figure 5.

Experiment Phase	T°C condition	Crystalline products	Composition %wt							Position in the diagram		
			Na ₂ O	MgO	Al ₂ O ₃	SiO ₂	K ₂ O	CaO	Total	Kls	Nph	Di
k402												
Melt	1,100	Omp+Kls+Nph+Spl	8.31	1.28	28.81	45.83	14.07	1.69	100.00	47.49	42.65	9.86
STD			0.15	0.01	0.06	0.10	0.15	0.01				
Omp (Di76Jd24)			3.49	8.82	25.31	39.79	0.22	22.36	100.00			
STD			0.20	0.54	3.04	2.22	0.17	0.35				
Kls			5.15	0.01	35.55	34.53	24.69	0.07	100.00			
STD			0.03	0.02	0.06	0.06	0.07	0.05				
Nph			13.27	0.02	37.11	36.14	13.25	0.22	100.00			
STD			0.09	0.02	0.06	0.06	0.07	0.02				
Spl			0.02	29.25	70.41	0.25	0.06	0.02	100.00			
STD			0.02	0.08	0.08	0.12	0.03	0.02				
k403												
Melt	1,100	Di+Kls+Crn	1.21	0.85	23.90	54.21	18.87	0.95	100.00	83.90	8.14	7.96
STD			0.05	0.29	0.96	1.67	0.67	0.54				
Di (Di93Jd7)			0.99	15.73	7.89	50.32	0.24	24.83	100.00			
STD			0.15	0.61	1.02	0.43	0.25	0.42				
Kls			1.47	0.23	32.81	38.71	26.43	0.36	100.00			
STD			0.07	0.15	0.34	0.30	0.37	0.13				
Crn			0.18	0.39	96.16	2.06	1.08	0.09	100.00			
STD			0.02	0.04	1.58	0.87	0.67	0.04				
k404												
Melt	1,300	Di	2.92	4.59	23.75	47.46	14.65	6.63	100.00	48.81	14.76	36.42
STD			0.02	0.25	0.41	0.03	0.24	0.41				
Di (Di96Jd4)			0.61	14.14	13.73	46.37	0.07	25.08	100.00			
STD			0.03	0.28	0.64	0.36	0.04	0.11				
k405												
Melt	1,300	Di	12.71	4.43	25.35	48.01	4.15	5.35	100.00	12.53	58.29	29.18
STD			0.39	0.16	0.92	0.16	0.39	1.03				
Di (Di87Jd13)			1.83	14.36	11.09	49.29	0.01	23.41	100.00			
STD			0.16	0.77	1.55	0.80	0.01	0.20				

STD: standard deviation; Omp: omphacite; Crn: corundum; Spl: spinel.

Point 403 defines a pseudo-peritectic in which Kls + San + (Di₉₀Jd₁₀) + Wo and liquid (Lct₇₆Nph₁₈Di₆) are in equilibrium at 1,200°C (Figure 3D). In this experiment, Wo and Di formed agglomeration of crystals, which makes them indistinguishable in the back-scattered electron (BSE) image, but both were clearly detected by the XRD analyzes (Figure 4). Experiment 403 liquid phase composition had decreasing in the K₂O/Na₂O ratio in relation to the initial sample composition (K₂O/Na₂O = 4.75_{initial} → 3.2_{final}). This condition is buffered by simultaneous crystallization of two potassic phases: sanidine and kalsilite.

Experiment 406 (Lct₇₃Nph₁₈Di₉) is a pseudo-eutectic with liquid in equilibrium with Di+Kls+Wo at 1,000°C (Figure 3E). The position of this pseudo-eutectic point suggests a high thermal cotectic between experiments 402 and 406. Such high thermal is near 413 point (see figures 2 and 3B), that defines the impossibility of having both potassic/ultrapotassic and sodic magmas from the same metasomatic mantle source, subordinated to the Kls stability field presence. Liquid phase compositions of experiments 415, 402 and 413 show increasing in the K₂O/Na₂O ratio in relation to initial samples compositions (K₂O/Na₂O₍₄₁₅₎ = 0.28_{initial} → 0.37_{final}; K₂O/Na₂O₍₄₀₂₎ = 0.58_{initial} → 1.64_{final}; K₂O/Na₂O₍₄₁₃₎ = 1.17_{initial} → 1.82_{final}). This data shows that point 402 had the most expressive K₂O/Na₂O increasing, almost three times its initial value. In this experiment, Nph crystallization increased K₂O/Na₂O ratio, until K₂O concentration is enough to start kalsilite precipitation.

Wollastonite (CaSiO₃), a pyroxenoid that shows no solid solution with Di (Morimoto, 1989), occurred in experiments

406 and 403. This mineral can occur in several associations, but it is commonly found in metamorphic associations (e.g., limestones), or carbonatites (Greenwood, 1967; Klaudius and Keller, 2006). Some recent works point out its presence in alkaline silica-undersaturated rocks associations (Ruberti et al., 2012) and ijolites from Prairie Lake Carbonatite Complex (Canada) (Zurevinski and Mitchell, 2015). Wollastonite (CaSiO₃) is a low-pressure precursor of Ca-perovskites (Sueda et al., 2006). In our experiments, after Di crystallization to consume all available magnesium in the liquid, wollastonite is the natural Ca-rich crystallized phase.

Results for kalsilite-nepheline-diopside at 4.0 GPa and dry condition

Stability fields for Kls, Nph, and Cpx_{ss} (Di and Omp), together with a pseudo-eutectic point and cotectic lines, were determined in the Kls-Nph-Di system (Figure 5). Experimental conditions and products are given in Table 4.

The study of the Kls-Nph-Di system aims to test the effects of a more undersaturated composition in the previously determined mineral assemblage (Lct-Nph-Di system). As a result of the higher silica-undersaturation, Kls stability field expands, while the Nph field retracts. In such way, the pseudo-eutectic Lc₆₂Ne₂₉Di₉ (experiment 402, Figure 2) is shifted to a potassium poorer position Kls₄₇Nph₄₃Di₁₀ (experiment k402, Figure 5). This is buffered by the higher acceptance of potassium within Nph, in comparison to the values shown in the Lct-Nph-Di system (as well, inversely, lower acceptance of sodium in Kls). In this way, Nph acceptance of Kls compound has grown from 35 to 39 mol%, while Kls acceptance of Nph compound decreased from 27 to 24 mol%. As expected, olivine did not appear in this system, due to the restriction imposed by high alkaline concentration, in agreement with data obtained here for the Lct-Nph-Di system.

The piercing point k402 is a pseudo-eutectic, with Kls + Nph + Omp ± Spl (spinel) crystalline phases in equilibrium with a liquid (Kls₄₇Nph₄₃Di₁₀) at 1,100°C. Nph, Omp (Di₇₆Jd₂₄), and Spl are euhedral (Figure 6A). In experiment k403, a very small amount of corundum (Crn) occurred in equilibrium with Kls+Di plus liquid (Kls₈₄Nph₈Di₈) at 1,100°C.

PETROLOGIC IMPLICATIONS

Gupta et al. (2006) show that nephelinite and phonolite compositions could be represented on the San-Nph-Di plane at 1.0 and 2.0 GPa. In the present work, we used Lct-Nph-Di and Kls-Nph-Di systems at 4.0 GPa, more silica-undersaturated than the system studied in the cited reference, to represent more primitive environments and strongly emphasize the differences between sodic and potassic primitive liquids. Nephelinites and nepheline syenites (and their volcanic equivalents) are

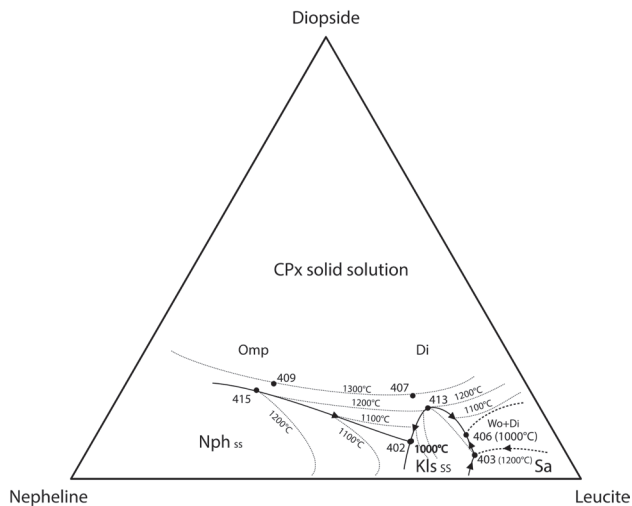


Figure 2. Leucite-nepheline-diopside (Lct-Nph-Di) phase diagram at 4 GPa and dry conditions. Kalsilite (Kls_{ss}), Nepheline (Nph_{ss}), sanidine (Sa), clinopyroxene (Cpx_{ss}) and wollastonite (Wo) stability fields are shown in the diagram. Experiment 402 (Kls + Nph + Di), 403 (Kls + Sa + Di) and 406 (Kls + Wo + Di) are piercing points. Solid and dashed lines are determined and inferred cotectic lines, respectively. Point 413 is a thermal high, defining a boundary between the ultrapotassic (to its right side) and potassic to sodic (to its left side) stability fields.

commonly represented by Nph + Cpx + Kfs (K-feldspar, usually Sa) assemblage (Gupta et al., 2006). However, at 4.0 GPa (~120 km deep) kalsilite became stable, and its presence created a thermal barrier (thermal high in experiment 413, Figure 2) between the Sa and Nph fields. Without an eutectic in equilibrium

with Nph + Sa, nephelinites and nepheline syenites assemblages cannot be produced during a rock crystallization path.

K-rich mineral stability studies are not conclusive about what the best mineral acting as potassium reservoir in mantelic environment is. Liu (1987) argue that wadeite-type $K_2Si_4O_9$,

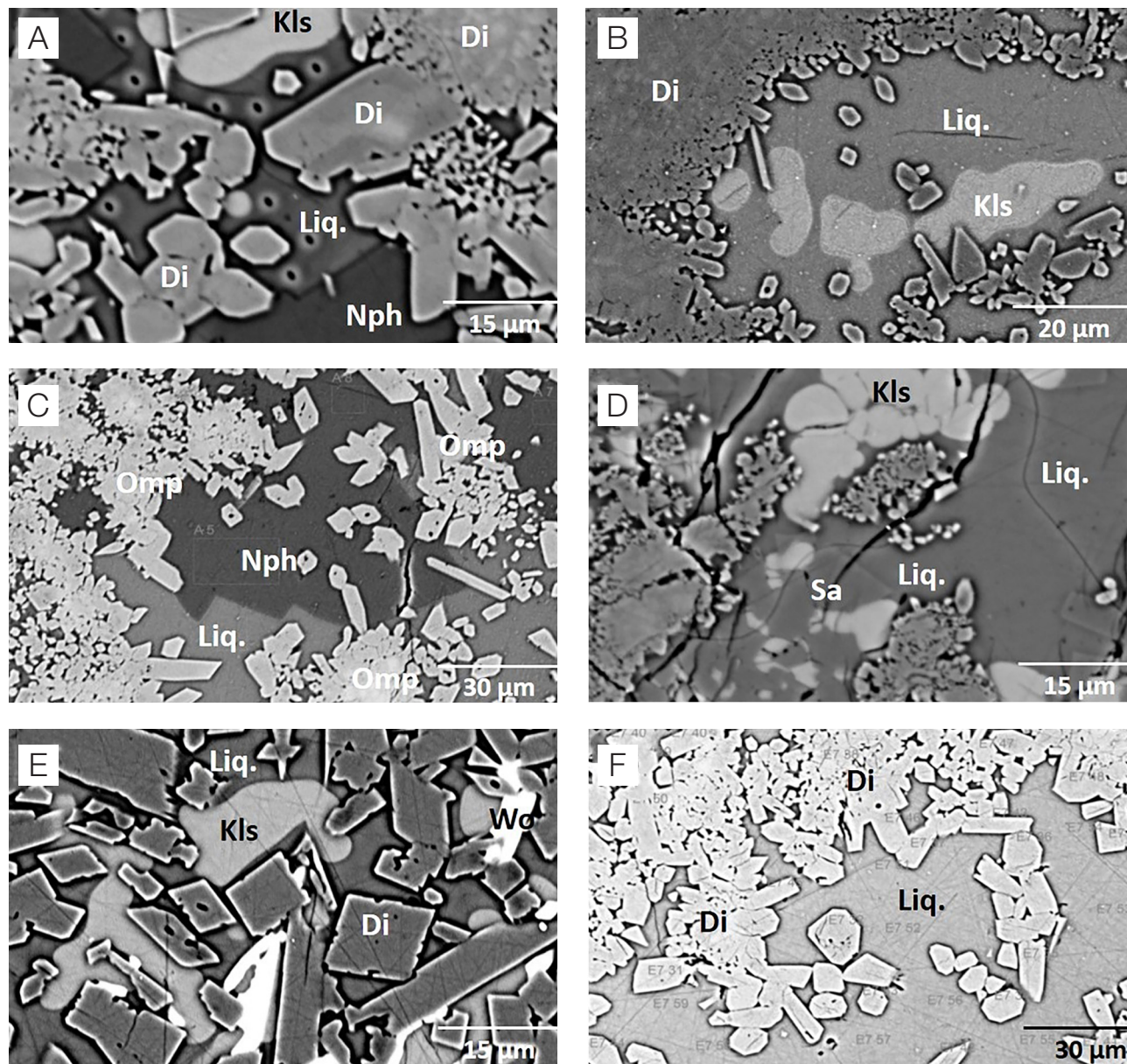


Figure 3. Back-scattered electron (BSE) images of some experiments for the leucite-nepheline-diopside (Lct-Nph-Di) system: (A) pseudo-eutectic four-phase point (402) with kalsilite + nepheline + diopside (Kls + Nph + Di) crystalline phases plus liquid ($Lc_{62}Ne_{29}Di_9$) at 1,000°C; (B) experiment 413 with Di + Kls in equilibrium with a liquid ($Lct_{62}Nph_{21}Di_{17}$); (C) experiment 415 with omphacite + nepheline (Omp + Nph) in equilibrium with liquid ($Lct_{29}Nph_{50}Di_{21}$) at 1,200°C; (D) four-phase pseudo-peritectic point (experiment 403) with kalsilite + sanidine + (diopside + wollastonite) [Kls + Sa + (Di + Wo)] crystalline phases in equilibrium with liquid ($Lct_{75}Nph_{22}Di_2$), Di and Wo occurs like agglomerates of small crystals, and its members are not quite well distinguished by imaging BSE for this experiment; (E) four phase pseudo-eutectic point (experiment 406) with Kls + Di + Wo in equilibrium with liquid ($Lct_{74}Nph_{17}Di_9$), Kls is always close to Wo crystals; (F) experiment 407 is an example of two-phase point, as experiments 404, 405 and 409.

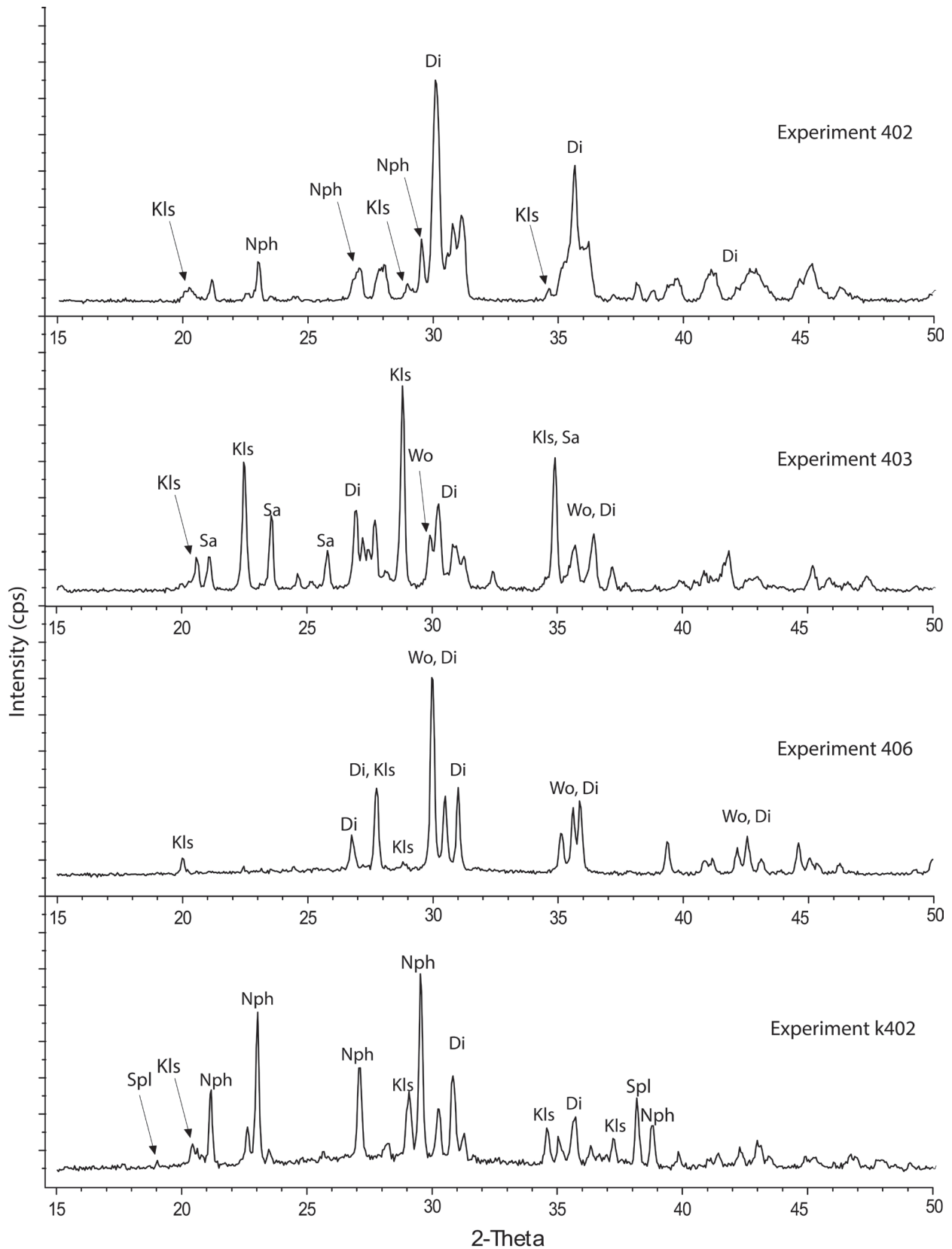


Figure 4. X-ray diffraction (XRD) analysis for the four-phase points of the leucite-nepheline-diopside (Lct-Nph-Di) (experiments 402, 403 and 406), and the kalsilite + nepheline + diopside (Kls + Nph + Di) (experiment 402) systems.

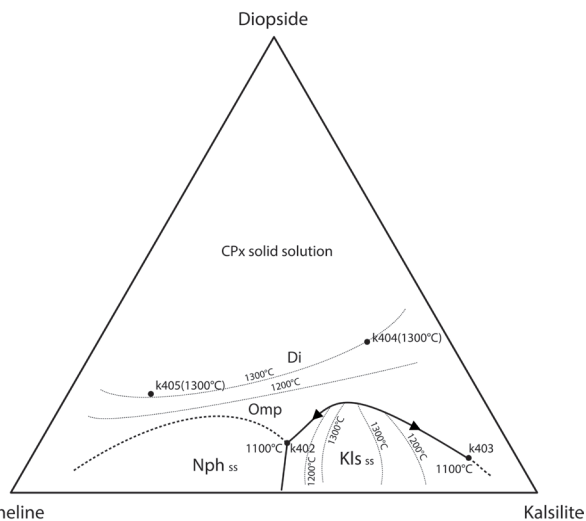


Figure 5. Kalsilite + nepheline + diopside (Kls + Nph + Di) phase diagram at 4 GPa and dry conditions. Kls_{ss}, Nph_{ss} and clinopyroxene (Cpx_{ss}) stability fields are shown in the diagram. Experiment 402 is a pseudo-eutectic point with Kls + Nph + Di + (spinel), in equilibrium with liquid (Kls₄₇Nph₄₃Di₁₀) at 1,100°C. Solid and dashed lines are defined and inferred cotectic lines, respectively.

is a more plausible potassic phase at pressures higher than 5 GPa due to its octahedral structure. Wendlandt and Eggler (1980) affirm that kalsilite is more stable than sanidine in depths higher than 100 km (~3.5 GPa), while in recently data Hirao et al. (2008) shows K-feldspar stability up to ~8 GPa and 1,000°C. Our data (at 4.0 GPa) verify Kls in equilibrium with Nph + Di (1,000°C), Sa + Di (1,200°C) and Di (1,200°C). As clinopyroxene is a common mantle mineral, the assemblage Di + Kls suggests that kalsilite can be an important k-rich phase capable of carry potassium to deeper portions of the mantle, corroborating with Wendlandt and Eggler (1980) data.

Influence of alkalis in silica activity

Figure 7 shows binary plots comparing alkali and silica wt% of both experimental (present study) and natural compositions of alkaline silica-undersaturated rocks from various locations around the world (Comin-Chiaramonti et al., 1997; Zhu et al., 2016; Konopelko et al., 2014). Silica enrichment in low-degree melts of lherzolites has been observed in experimental studies, mainly because of high concentration of alkalis, which depolymerizes the liquid and decreases its silica activity (Laporte

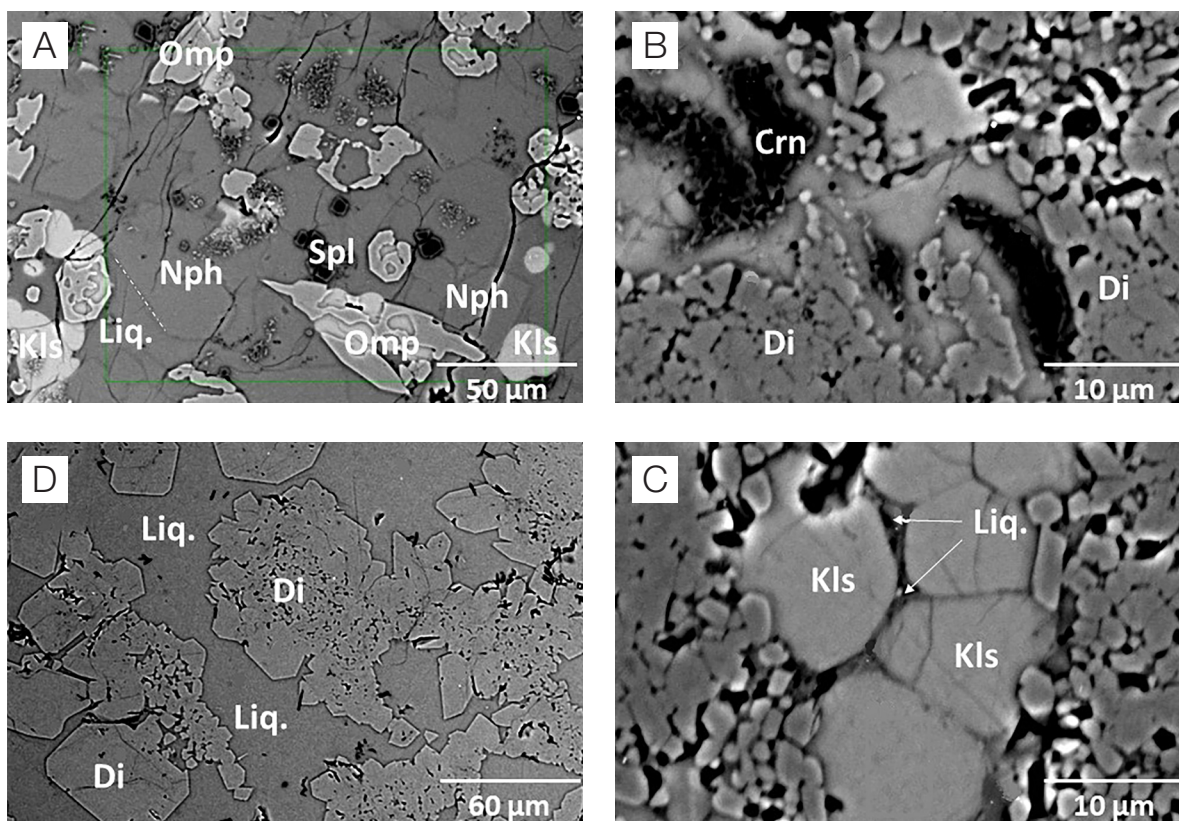


Figure 6. Back-scattered electron (BSE) images of experiments runs for kalsilite-nepheline-diopside (Kls-Nph-Di) system: (A) experiment k402 is a pseudo-eutectic point with kalsilite + nepheline + omphacite (Kls + Nph + Omp) (presence of spinel) plus a liquid (Kls₄₇Nph₄₃Di₁₀) at 1,100°C; (B) experiment k403 with Kls+Di (in the presence of corundum) plus a liquid (Kls₈₄Nph₈Di₈) at 1,100°C; (C) detail on experiment k403, showing liquid in the interstices of Kls; (D) the two phase experiments k404 and k405, both at 1,300°C.

et al., 2014). The depolymerization effect has to be compensated by the increasing of SiO₂ wt% in the melt (Ryerson, 1985). This effect was documented up to 3.0 GPa (Davis and Hirschmann, 2013), but our data extend it to at least 4.0 GPa.

Our data suggest positive correlations between K₂O wt% and silica concentration in magmas sources (Figure 7A), in agreement with Conceição and Green (2000, 2004). However, sodium concentration did not show uniform correlation with SiO₂ wt% in our data or natural occurrences (Figure 7B). In such way, sodium correlation with silica has to be dependent on other factors (pressure, temperature or mineralogical assemblages). Calcium showed negative correlation with SiO₂ wt% in the experiments and natural data (Figure 7C). As calcium is more compatible than the other alkaline elements, its correlation with silica seems to be dependent on the degree of melting of the magma source. It suggests that higher and lower concentrations of calcium reflect higher and lower degrees of melting in the source of magmas, respectively.

CONCLUSIONS

With the study of the Lct-Nph-Di system at 4.0 GPa and dry conditions, we establish the stability fields for Kls_{ss}, Nph_{ss} and CPx_{ss} solid solutions, plus Wo and Sa. Three piercing points were determined in this system:

- experiment 402: a pseudo-eutectic with Kls+Nph+Di crystalline phases in equilibrium with liquid (Lc₆₂Ne₂₉Di₉) at 1,000°C;
- experiment 403: a piercing point with Kls+Sa+Di+Wo in equilibrium with liquid (Lct₇₅Nph₂₂Di₂) at 1,200°C;
- experiment 406: another pseudo-eutectic with Kls+Di+Wo in equilibrium with liquid (Lct₇₄Nph₁₇Di₉) at 1,000°C.

Point 413 (Lct₆₂Nph₂₁Di₁₇) is a thermal high that prevents sodic and potassic/ultrapotassic magmas from the same mantle source. With the Kls-Nph-Di plane, we determined the stability fields for Kls_{ss}, Nph_{ss} and Cpx_{ss}. This plane has a pseudo-eutectic with Kls+Nph+Di+(Spl) in equilibrium with liquid (Kls₄₇Nph₄₃Di₁₀) at 1,100°C.

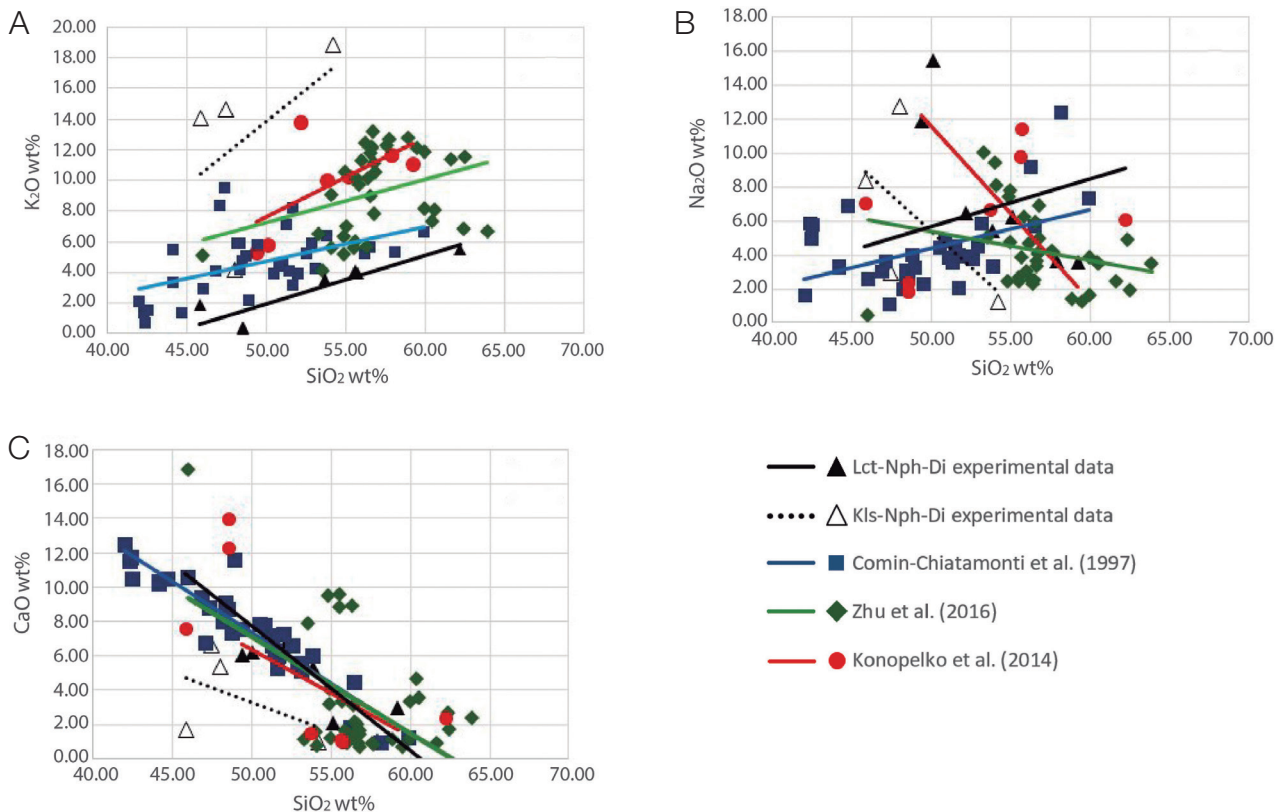


Figure 7. Binary plots (oxide wt%) between alkali (K₂O, Na₂O and CaO) and SiO₂ wt%. Experimental data are composition of liquids in equilibrium from leucite-nepheline-diopside (Lct-Nph-Di) and kalsilite + nepheline + diopside (Kls + Nph + Di) systems, represented by solid and open triangles. Other data represent groups of alkaline rocks related in formation around the world: solid squares for phonolites, tephrites, nephelinites and gabbros from eastern Paraguay (Comin-Chiaramonti et al., 1997), solid circles for syenites, trachytes and phonolites from NE China (Zhu et al., 2016); and solid diamonds for gabbros and syenites from central Kyrgyzstan (Konopelko et al., 2014). Trendlines shows positive (K₂O), irregular (Na₂O) and negative (CaO) relations between alkalis and SiO₂ wt%.

Our data suggest that, in more silica-undersaturated systems, Kls dissolution in Nph is higher, up to 35 (in Lct-Nph-Di) and 39 mol% (in Kls-Nph-Di), while Nph dissolution in Kls is up to 27 (in Lct-Nph-Di) and 24 mol% (in Kls-Nph-Di). The solubility of Kls in Nph_{ss} and Nph in Kls_{ss} is determinant to the position of the pseudo-eutectic Nph+Kls+Cpx+liquid (point 402 in the Lct-Nph-Di plane, and k402 in the Kls-Nph-Di plane). The richer the Nph is in K, the more prominent the shift of the pseudo eutectic is towards a Na richer field of the diagram. The opposite happens if Kls is Na-richer (the pseudo-eutectic is shifted to a potassium richer field).

In agreement with previous works, experimental data showed positive correlation between K₂O and SiO₂ wt% concentrations in the liquids in equilibrium with produced crystalline phases. However, Na₂O did not point out any correlation with SiO₂ contents, while Ca exhibited negative correlation with silica abundances in liquids.

REFERENCES

- Arevalo Jr., R., McDonough, W. F., Luong, M. (2009). The K/U ratio of the silicate Earth: insights into mantle composition, structure and thermal evolution. *Earth and Planetary Science Letters*, 278, 361-369. <http://dx.doi.org/10.1016/j.epsl.2008.12.023>
- Bea, F., Montero, P., Haissen, F., El Archi, A. (2013). 2.46 Ga kalsilite and nepheline syenites from the Awsard pluton, Reguibat Rise of the West African Craton, Morocco. Generation of extremely K-rich magmas at the Archean-Proterozoic transition. *Precambrian Research*, 224, 242-254.
- Carniel, L. C., Conceição, R. V., Dani, N., Stefani, V. F., Balzaretto, N. M., Reis, R. (2014). Structural changes of potassium-saturated smectite at high pressures and high temperatures: Application for subduction zones. *Applied Clay Science*, 102, 164-171. <https://doi.org/10.1016/j.clay.2014.09.037>
- Comin-Chiaramonti, P., Cundari, A., Piccirillo, M., Gomes, C. B., Castorina, F., Censi, P., De Min, A., Marzolini, A., Speziale, S., Velázquez, V. F. (1997). Potassic and Sodic Igneous Rocks from Eastern Paraguay: their Origin from the Lithospheric Mantle and Genetic Relationships with the Associated Paraná Flood Tholeiites. *Journal of Petrology*, 38, 495-528. <https://doi.org/10.1093/ptro/38.4.495>
- Conceição, R. V., Green, D. H. (2000). Behavior of the cotectic curve En-Ol in the system leucite - olivine - quartz under dry conditions to 2.0 GPa. *Geochemistry Geophysics Geosystems*, 1. <https://doi.org/10.1029/2000GC000071>
- Conceição, R. V., Green, D. H. (2004). Derivation of potassic (shoshonitic) magmas by decompression melting of phlogopite+pargasite lherzolite. *Lithos*, 72, 209-229. <http://dx.doi.org/10.1016/j.lithos.2003.09.003>
- Conceição, R. V., Nardi, L. V. S., Conceição, H. (2000). The Santanópolis syenite: genesis and evolution of Paleoproterozoic shoshonitic syenites in northeastern Brazil. *International Geology Review*, 42, 941-957. <https://doi.org/10.1080/00206810009465119>
- Condamine, P., Ménard, E. (2014). Experimental melting of phlogopite-bearing mantle at 1 GPa: Implications for potassic magmatism. *Earth and Planetary Science Letters*, 397, 80-92. <https://doi.org/10.1016/j.epsl.2014.04.027>
- Davis, F. A., Hirschmann, M. M. (2013). The effects of K₂O on the compositions of near-solidus melts of garnet peridotite at 3 GPa and the origin of basalts from enriched mantle. *Contributions to Mineralogy and Petrology*, 166, 1029-1046. <https://doi.org/10.1007/s00410-013-0907-0>
- Draper, D. S., Green, T. H. (1999). P, T phase relations of silicic, alkaline, aluminous liquids: new results and applications to mantle melting and metasomatism. *Earth and Planetary Science Letters*, 170, 255-268. [https://doi.org/10.1016/S0012-821X\(99\)00111-9](https://doi.org/10.1016/S0012-821X(99)00111-9)
- Edgar, A. D., Green, D. H., Hibberson, W. (1976). Experimental petrology of a highly potassic magma. *Journal of Petrology*, 17, 339-356. <https://doi.org/10.1093/ptrology/17.3.339>
- Foley, S. F., Venturelli, G., Green, D. H., Toscani, L. (1987). The ultrapotassic rocks: characteristics, classification and constraints for petrographic models. *Earth-Science Reviews*, 24, 81-134. [http://dx.doi.org/10.1016/0012-8252\(87\)90001-8](http://dx.doi.org/10.1016/0012-8252(87)90001-8)
- Greenwood, H. J. (1967). Wollastonite: stability in H₂O-CO₂ mixtures and occurrence in a contact-metamorphic aureole near Salmo, British Columbia, Canada. *American Mineralogist*, 52, 1669-1680.
- Gupta, A. K., Chattopadhyay, S., Chattopadhyay, B., Arima, M. (2006). Experimental study of the system diopside-nepheline-sanidine at 0.1, 1 and 2 GPa [P(H₂O)=P(Total)]: Its significance in the genesis of alkali-rich basic and ultrabasic rocks. *Lithos*, 86, 91-109. <http://dx.doi.org/10.1016/j.lithos.2005.04.005>
- Gupta, A. K., Dwivedi, M. M., Bhattachariya, H., Dasgupta, S. (2010). Silica-undersaturated portion of the system nepheline - kalsilite - SiO₂ at 2 GPa [P(H₂O) = P(total)]. *The Canadian Mineralogist*, 48, 1297-1313. <https://doi.org/10.3749/canmin.48.5.1297>

- Gupta, A. K., Green, D. H. (1988). The liquidus surface of the system forsterite – kalsilite – quartz at 28 kb under dry conditions, in presence of H₂O and CO₂. *Mineralogy and Petrology*, 39, 163-174. <https://doi.org/10.1007/BF01163032>
- Gupta, A. K., Lidiak, E. G. (1973). The System Diopside-Nepheline-Leucite. *Contributions to Mineralogy and Petrology*, 41, 231-239. <https://doi.org/10.1007/BF00371033>
- Hirao, N., Ohtani, E., Kondo, T., Sakai, T., Kikegawa, T. (2008). Hollandite II phase in KAlSi₃O₈ as a potential host mineral of potassium in the Earth's lower mantle. *Physics of the Earth and Planetary Interiors*, 166, 97-104. <http://dx.doi.org/10.1016/j.pepi.2007.11.002>
- Jaupart, C., Labrosse, S., Mareschal, J. C. (2007). Temperatures, heat and energy in the mantle of the Earth. In: G. Schubert (Ed.), *Treatise of Geophysics* (2nd edition, 223-270). Oxford: Elsevier.
- Klaudius, J., Keller, J. (2006). Peralkaline silicate lavas at Oldoinyo Lengai, Tanzania. *Lithos*, 91, 173-190. <http://dx.doi.org/10.1016/j.lithos.2006.03.017>
- Klein, C., Dutrow, B. (2007). *Manual of Mineral Science*. Michigan: Wiley.
- Konopelko, D., Biske, G., Seltmann, R., Petrov, S. P., Lepekthina, E. (2014). Age and petrogenesis of the Neoproterozoic Chon-Ashu alkaline complex, and a new discovery of chalcopyrite mineralization in the eastern Kyrgyz Tien Shan. *Ore Geology Reviews*, 61, 175-191. <https://doi.org/10.1016/j.oregeorev.2014.02.004>
- Laporte, D., Lambart, S., Schiano, P., Ottolini, L. (2014). Experimental derivation of nepheline syenite and phonolite liquids by partial melting of upper mantle peridotites. *Earth and Planetary Science Letters*, 404, 319-331. <http://dx.doi.org/10.1016/j.epsl.2014.08.002>
- Le Maitre, R. W. (2002). *Igneous Rocks: A classification and Glossary of terms*. New York: Cambridge University Press.
- Liu, L. G. (1987). High-pressure phase transitions of potassium aluminosilicates with an emphasis on leucite. *Contributions to Mineralogy and Petrology*, 95, 1-3. <https://doi.org/10.1007/BF00518025>
- Luth, R. W. (1997). Experimental study of the system phlogopite – diopside from 3.5 to 17 GPa. *American Mineralogist*, 82, 1198-1209. <http://dx.doi.org/10.2138/am-1997-11-1216>
- Lyubetskaya, T., Kurenaga, J. (2007). Chemical composition of Earth's primitive mantle and its variance: I. Method and results. *Journal of Geophysical Research*, 112, 1-21. <https://doi.org/10.1029/2005JB004223>
- McDonough, W. F., Sun, S. S. (1995). The composition of the Earth. *Chemical Geology*, 120, 223-253. [https://doi.org/10.1016/0009-2541\(94\)00140-4](https://doi.org/10.1016/0009-2541(94)00140-4)
- Mengel, K., Green, D. H. (1989). Stability of amphibole and phlogopite in metasomatized peridotite under water-saturated and water-undersaturated conditions. *IV International Kimberlite Conference, Annals*, 14, 571-581. Perth.
- Menzies, M. A., Hawkesworth, C. J. (1987) Mantle Metasomatism. In: M. A. Menzies, N. Rogers, A. Tindle, C. J. Hawkesworth (Eds.), *Metasomatic and enrichment processes in lithospheric peridotites, an effect of asthenosphere-lithosphere interaction* (v. 125, 313-361). London: University of London Academic Press.
- Morimoto, N. (1989). Nomenclature of Pyroxenes. *Mineralogical Journal*, 14(5), 198-221.
- Plá Cid, J., Nardi, L. V. S., Plá Cid, C., Gisbert, P. E., Balzaretto, N. M. (2014). Acid compositions in a veined-lower mantle, as indicated by inclusions of (K,Na)-Hollandite + SiO₂ in diamonds. *Lithos*, 196-197, 42-53. <http://dx.doi.org/10.1016/j.lithos.2014.02.019>
- Ryerson, F. J. (1985). Oxide solution mechanisms in silicate melts: Systematic Variations in the activity coefficient of SiO₂. *Geochimica et Cosmochimica Acta*, 49, 637-649. [https://doi.org/10.1016/0016-7037\(85\)90159-0](https://doi.org/10.1016/0016-7037(85)90159-0)
- Ruberti, E., Enrich, G. E. R., Azzone, R. G., Comin-Chiaromonte, P., De Min, A., Gomes, C. B. (2012). The Banhadão Alkaline Complex, Southeastern Brazil: source and evolution of potassic SiO₂-undersaturated high-Ca and low-Ca magmatic series. *Mineralogy and Petrology*, 104, 63-80. <https://doi.org/10.1007/s00710-011-0171-9>
- Schairer, J. F. (1950). The albite-feldspar join in the system NaAlSi₃O₈-KAlSi₃O₈-SiO₂. *Journal of Geology*, 58, 512-517.
- Singh, P., Arima, M., Gupta, A. K. (2000). Phase equilibrium constraints on the petrogenesis of nephelinites with reference to the system diopside–nepheline under variable P–T conditions in the presence or absence of water. *Journal of Mineralogical and Petrological Sciences*, 95, 113-124. <https://doi.org/10.2465/jmps.95.113>

- Sood, M. K., Platt, R. G., Edgar, A. D. (1970). Phase relations in portions of the system diopside-nepheline-kalsilite-silica end their importance in the genesis of alkaline rocks. *The Canadian Mineralogist*, 10(3), 380-394.
- Sueda, Y., Irifune, T., Yamada, A., Inoue, T., Liu, X., Funakoshi, K. (2006). The phase boundary between, CaSiO₃ perovskite and Ca₂SiO₄ + CaSi₂O₅ determined by in situ X-ray observations. *Geophysical Research Letters*, 33, L10307. <https://doi.org/10.1029/2006GL025772>
- Wallace, M. E., Green, D. H. (1991). The effect of bulk rock compositions on the stability of amphibole in the upper mantle: implications for solidus positions and mantle metasomatism. *Mineralogy and Petrology*, 44, 1-19. <https://doi.org/10.1007/BF01167097>
- Walter, M. J., Presnall, D. C. (1994). Melting behavior of simplified lherzolite in the system CaO–MgO–Al₂O₃–SiO₂–Na₂O from 7 to 35 kbar. *Journal of Petrology*, 35, 329-359. <https://doi.org/10.1093/petrology/35.2.329>
- Wendlandt, R. F., Eggler, D. H. (1980). The origins of potassic magmas: I. melting relations in the systems KAlSiO₄-Mg₂SiO₄-SiO₂ and KAlSiO₄-MgO-SiO₂-CO₂ to 30 kilobars. *American Journal of Science*, 280, 385-420. <https://doi.org/10.2475/ajs.280.5.385>
- Whitney, D. L., Evans, B. W. (2010). Abbreviations for names of rock forming minerals. *American Mineralogist*, 95, 185-187. <https://doi.org/10.2138/am.2010.3371>
- Yoder, H. S., Tilley, C. E. (1962). Origin of basalt magmas: an experimental study of the natural and synthetic rock systems. *Journal of Petrology*, 3, 342-532. <https://doi.org/10.1093/petrology/3.3.342>
- Zhu, Y. S., Yang, J. H., Sun, J. F., Zhang, J. H., Wu, F. Y. (2016). Petrogenesis of coeval silica-saturated and silica-undersaturated alkaline rocks: Mineralogical and geochemical evidence from the Saima alkaline complex, NE China. *Journal of Asian Earth Science*, 117, 184-207. <https://doi.org/10.1016/j.jseaes.2015.12.014>
- Zurevinski, S. E., Mitchell, R. H. (2015). Petrogenesis of orbicular ijolites from the Prairie Lake complex, Marathon, Ontario: Textural evidence from rare processes of carbonatitic magmatism. *Lithos*, 239, 234-244. <https://doi.org/10.1016/j.lithos.2015.11.003>